Electronic structure of tetragonal $LaCuO_3$ studied by photoemission and x-ray-absorption spectroscopy

T. Mizokawa and A. Fujimori
Department of Physics, University of Tokyo, Bunkyo-ku, Tokyo 113, Japan

H. Namatame
Department of Material Science, University of Hiroshima, Kagamiyama 1-3, Higashi-Hiroshima 724, Japan

Y. Takeda
Department of Chemistry, Faculty of Engineering, Mie University, Tsu 154, Japan

M. Takano
Institute for Chemical Research, Kyoto University, Uji, Kyoto 611, Japan

(Received 2 September 1997)

The electronic structure of the formally Cu^{3+} metallic $LaCuO_3$ has been studied by photoemission and x-ray-absorption spectroscopy. By analyzing the valence-band and Cu $2p$ core-level photoemission spectra using a CuO_6 cluster model, the charge-transfer energy is estimated to be -1 eV, indicating that the ground state is dominated by the $d^9\underline{L}$ configuration with which the d^8 configuration is strongly hybridized, where $\underline{L}$ denotes a ligand hole. However, agreement between the experimental results and the cluster-model calculations is not satisfactory for the detailed line shape of the main peaks. Especially, the Cu $2p$ x-ray-absorption spectrum cannot be well explained by the single-site cluster-model calculation, suggesting the importance of intercluster interaction. On the other hand, the existence of the charge-transfer satellite in the Pauli-paramagnetic state is explained by Hartree-Fock band-structure and self-energy calculations using parameters deduced from the analysis of the photoemission spectra.
[S0163-1829(98)00315-4]

I. INTRODUCTION

Since the discovery of the high-T_c copper oxides,[1] the electronic structure of the hole-doped Cu^{2+} oxides has been subject to extensive investigations. X-ray-absorption and photoemission studies on the high-T_c cuprates have revealed that the doped holes mainly go into the O $2p$ orbitals.[2–4] Formally Cu^{3+} oxides such as $NaCuO_2$ and $LaCuO_3$ have been frequently used as reference compounds in discussing the existence of Cu^{3+} species in the high-T_c cuprates.[5,6] On the other hand, the electronic structure of the formally Cu^{3+} oxides, which can be viewed as 100% hole-doped Cu^{2+} oxides, has attracted interest because it remains to be clarified whether the ground states are dominated by d^8 (real Cu^{3+}) or $d^9\underline{L}$ (formally Cu^{3+} but actually Cu^{2+} plus an oxygen p hole $\underline{L}$). If the latter is the case, the description of the electronic structures of such insulating and metallic states provides us with a challenging problem. One such compound, $NaCuO_2$, has been studied by photoemission spectroscopy and cluster-model analysis and has been found to have a ground state of $d^9\underline{L}$ character with which d^8 character is heavily mixed.[7] We have argued that in a compound with this type of ground state the magnitude of the band gap is determined by the relative strength of the hybridization within the local CuO_n cluster and that between the clusters.[7] $NaCuO_2$, which has a 90° Cu-O-Cu bond angle, is insulating because the band gap opens due to the strong Cu $3d-$O $2p$ hybridization within the CuO_4 cluster and the intercluster interaction is weak. On the other hand, in $LaCuO_3$ with a perovskite-type structure, which has an almost 180° Cu-O-Cu bond angle, the intercluster interaction is expected to be strong.

For $LaCuO_3$, two types of crystal structures have been reported: a rhombohedrally distorted perovskite structure synthesized at higher oxygen pressure[8] and a tetragonally distorted perovskite structure synthesized at lower oxygen pressure.[9] Both the rhombohedral and tetragonal $LaCuO_3$ have been found to be a poor metal,[8,10] whereas it has also been reported that the stoichiometric tetragonal $LaCuO_3$ shows a semiconducting behavior.[11] Band-structure calculations using the local-density approximation (LDA) predict $LaCuO_3$ to be a Pauli-paramagnetic metal.[12,13] Based on the LDA+U calculation, which predicts $LaCuO_3$ to be an antiferromagnetic (AFM) insulator, Czyzyk and Sawatzky[12] have claimed that the tetragonal $LaCuO_3$ is a semiconductor for the ideal stoichiometry and that its metallic behavior is derived from the oxygen deficiency. Few high-energy spectroscopic experiments such as photoemission spectroscopy, which provide important information on the electronic structure, have been reported. In this paper, we present photoemission and x-ray-absorption spectra of tetragonal $LaCuO_3$, which is almost stoichiometric and metallic. We have analyzed the spectra by the configuration-interaction (CI) cluster-model analysis and have extracted the electronic-structure parameters. Using the parameters deduced from the cluster-model analysis, we have performed unrestricted Hartree-Fock (HF) and subsequent self-energy correction

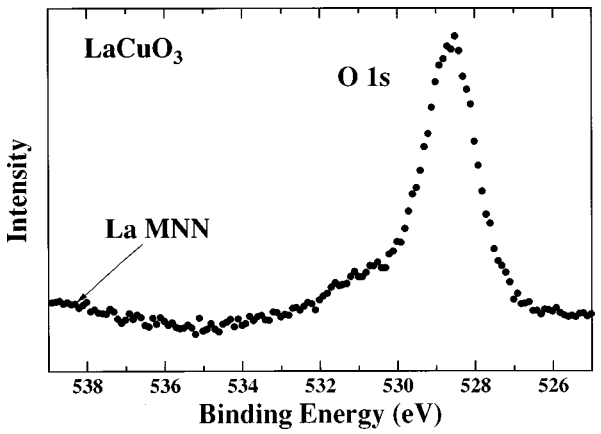

FIG. 1. O 1s XPS spectrum of $LaCuO_3$.

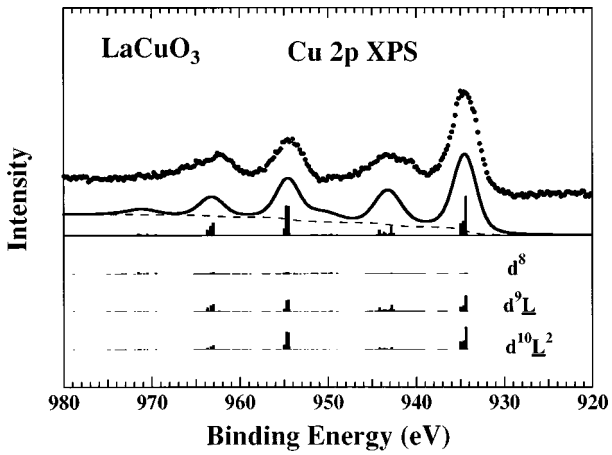

FIG. 2. Cu 2p core-level spectrum of $LaCuO_3$ compared with the CI cluster-model calculation (upper panel). Decomposition of the line spectra into final-state configurations is shown in the lower panel.

calculations on a Cu $3d-$O $2p$ lattice model in order to explain the photoemission spectra of Pauli-paramagnetic $LaCuO_3$. We have also analyzed the Cu 2p x-ray-absorption spectra in order to study how the intercluster interaction manifests itself in high-energy spectroscopy.

II. EXPERIMENT

Polycrystalline samples of $LaCuO_3$ were prepared by the following procedure. A mixture of La_2O_3 and CuO was pressed into a pellet and fired at 850 °C for 2–3 h in air. The product was milled and pressed into a pellet again. After firing at 1000 °C in air for 24 h, $LaCuO_{2.5}$ was obtained. The sample was further fired at 800 °C and 200 atoms for 48 h and at 400 °C and 400–500 atoms for 3–4 in an O_2 gas flow. Stoichiometry of the compounds was established by iodometric titrations as $LaCuO_{2.97\pm0.02}$. The samples show metallic and Pauli-paramagnetic behaviors.[10]

A Mg $K\alpha$ source ($h\nu=1253.6$ eV) was used for x-ray photoemission spectroscopy (XPS). XPS spectra were corrected for the Mg $K\alpha_{3,4}$ ghost. Photoelectrons were collected with a PHI double-pass cylindrical-mirror analyzer. The resolution including both the source width and the instrumental broadening was ~1.0 eV for XPS. Ultraviolet photoemission spectroscopy (UPS) spectra were measured at beamline BL-2 of the Synchrotron Radiation Laboratory, Institute for Solid State Physics, University of Tokyo. The energy resolution was 0.3–0.5 eV for photon energies ranging from 40 to 100 eV. The Fermi level was determined by evaporating Au on the sample. The binding energy in XPS was calibrated using the Au $4f_{7/2}$ peak at 84.0 eV. In order to prevent possible loss of oxygen atoms from the surface, the samples were cooled to liquid-nitrogen temperature (LNT) during the measurements. X-ray-absorption spectroscopy (XAS) was done at beamline BL-2B of Photon Factory, Laboratory for High Energy Physics. The energy resolution was ~0.2 eV at 530 eV. The photon energy was calibrated using the O 1s edge of TiO_2 at 530.7 eV (Ref. 14) and the Cu $2p_{3/2}$ edge of Cu metal at 932.5 eV.[15] The XAS spectra were taken at room temperature (RT) in the total electron yield method. In order to obtain fresh, clean surfaces, the samples were scraped *in situ* with a diamond file. The O 1s core-level spectrum became almost a single peak by scraping both at RT and at LNT (Fig. 1), which is an indication of good sample quality. The shoulder at ~531 eV may be due to surface contamination. Since the amount of the shoulder is less than 10% of the O 1s peak, the surface contamination does not affect the following cluster-model analyses of core-level spectra. The base pressure in the spectrometer was in the low 10^{-10}-torr range for XPS and UPS and was ~1 $\times10^{-9}$ torr for XAS.

III. RESULTS AND DISCUSSIONS

A. Core-level XPS

The Cu 2p core-level XPS spectrum is shown in Fig. 2. The binding energy of the Cu $2p_{3/2}$ peak is 934.5 eV, which is ~1 eV higher than that of CuO and is ~2 eV higher that those of Cu_2O and Cu metal.[16] The Cu 2p spectrum has satellite structures, which have generally been observed in late transition-metal oxides. Therefore, we have applied the CI cluster-model analysis including the multiplet effect.[17,18] Since in tetragonal $LaCuO_3$ there are four in-plane Cu-O bonds of 1.909 Å and two apical Cu-O bonds of 1.986 Å,[10] we have employed an elongated octahedral CuO_6 cluster with D_{4h} symmetry. The wave function of the ground state is given by a linear combination of d^8, $d^9\underline{L}$, and $d^{10}\underline{L}^2$ configurations, where $\underline{L}$ represents an oxygen 2p hole. The O 2p to Cu 3d charge-transfer energy Δ is defined by $\Delta \equiv E(d^9\underline{L})-E(d^8)$ and the 3d-3d Coulomb interaction energy by $U\equiv E(d^9)+E(d^7)-2E(d^8)$, where $E(d^n\underline{L}^m)$ is the center of gravity of the $d^n\underline{L}^m$ multiplet. The transfer integrals between the Cu 3d and O 2p orbitals are expressed in terms of Slater-Koster parameters $(pd\sigma)$ and $(pd\pi)$.[19] The ratio $(pd\sigma)/(pd\pi)$ is fixed at ~-2.2.[20,21] The transfer integrals between the O 2p orbitals are given by $(pp\sigma)$ and $(pp\pi)$, which are fixed at 0.60 and -0.15 eV, respectively. In addition, we have scaled the transfer integrals following Harrison's rule, which predicts the dependence of the transfer integrals on the interatomic distance.[21] The value of $(pd\sigma)$ given below is for the in-plane Cu-O bond. The multiplet coupling between the 3d electrons is included through Racah parameters B and C, which are fixed at 0.150 and 0.667 eV, namely, ~80% of the atomic HF values.[22] The wave func-

tions of the final states are given by linear combinations of $\underline{c}d^8$, $\underline{c}d^9\underline{L}$, and $\underline{c}d^{10}\underline{L}^2$ configurations, where $\underline{c}$ denotes a Cu $2p$ core hole. The multiplet coupling between the Cu $2p$ core hole and Cu $3d$ electrons is expressed in terms of Slater integrals F^2, G^1, and G^3, which are also fixed at 7.08, 5.37, and 3.06 eV, namely, ~80% of the atomic HF values.[18,22] In the cluster-model analysis of the Cu $2p$ XPS, we have four adjustable parameters: Δ, U, $(pd\sigma)$, and the multiplet-averaged $2p$-$3d$ Coulomb interaction $Q[\equiv F^0-(1/15)G^1-(3/70)G^3]$.

Here, we have fixed U and Q at 7.0 and 9.0 eV, respectively, which are close to the values obtained commonly in the cluster-model analyses of the late transition-metal oxides.[18,23] The best fit is obtained for $\Delta=-1.0\pm1.0$ eV and $(pd\sigma)=-1.7\pm0.2$ eV as shown in Fig. 2. The energy separation and relative intensity between the main and satellite structures are reproduced. The ground state is the high-spin state with ${}^3B_{1g}$ symmetry as in the cubic cluster because the elongation of the octahedra or the ratio of the apical Cu-O bond length to the in-plane one ~1.04 is too small. In order to stabilize the low-spin state compared with the high-spin state, the ratio is required to be larger than 1.13 with the best-fit parameter set. The ground state has 37% d^8, 53% $d^9\underline{L}$, and 10% $d^{10}\underline{L}^2$ characters. The final states are decomposed into the $\underline{c}d^8$, $\underline{c}d^9\underline{L}$, and $\underline{c}d^{10}\underline{L}^2$ components in the lower panel of Fig. 2. The main peaks have predominantly both $\underline{c}d^{10}\underline{L}^2$ and $\underline{c}d^9\underline{L}$ character and the satellite structures have $\underline{c}d^9\underline{L}$ character. In the ground state, the net number of the $3d$ holes is 1.27, which is close to the ionic value of Cu^{2+} rather than Cu^{3+}. In this sense, the electronic structure of $LaCuO_3$ given by the single-site cluster model is similar to that of $NaCuO_2$.[7] However, it is expected that the intercluster interaction is important in $LaCuO_3$, which has an almost 180° Cu-O-Cu bond. Actually, the asymmetric line shape of the main peak cannot be explained by the single cluster-model calculation as the other Cu oxides such as La_2CuO_4, which may be due to the intercluster interaction beyond the single-site cluster model.[24] The Cu $2p$ XPS spectrum of $LaCuO_3$ should be further investigated by a model including the intercluster interaction.

B. Valence band

The valence-band photoemission spectra taken at various photon energies from 40 to 1253.6 eV are displayed in Fig. 3. Since the relative photoionization cross section of O $2p$ to Cu $3d$ increases as the photon energy decreases, the structures at 3 and 5 eV mainly have the O $2p$ and Cu $3d$ characters, respectively. In the UPS spectrum taken at $h\nu=90$ eV, the existence of the satellite structure located at ~12 eV is clear. The satellite region from 9 to 13 eV is strongly enhanced and the main-band region from 0 to 7 eV is not enhanced by the $3p$-$3d$ resonance ($h\nu=74$ eV: on resonance; $h\nu=70$ eV: off resonance), indicating that the satellite can be regarded as a so-called charge-transfer satellite.

The calculated line spectra with $\Delta=-1.0$ eV, $U=7.0$ eV, and $(pd\sigma)=-1.7$ eV have been broadened with a Gaussian and a Lorentzian and are compared with the valence-band XPS spectrum in Fig. 4. The full width at half maximum (FWHM) of the Gaussian is ~1.0 eV, which is mainly determined by the energy resolution of the analyzer, and that of the Lorentzian is $\sim0.4+0.3E_B$ eV, where the first term is derived from the natural width of the x-ray source and the second term proportional to the binding energy E_B is from the lifetime of the final states. The satellite structure, whose existence becomes clear by subtracting the background due to secondary electrons, is well reproduced. Here, we have added the contribution from the O $2p$ band of a Gaussian form centered at ~3 eV whose relative cross section to the Cu $3d$ band is assumed to be three times larger than that of the atomic calculation.[25] From the cluster-model

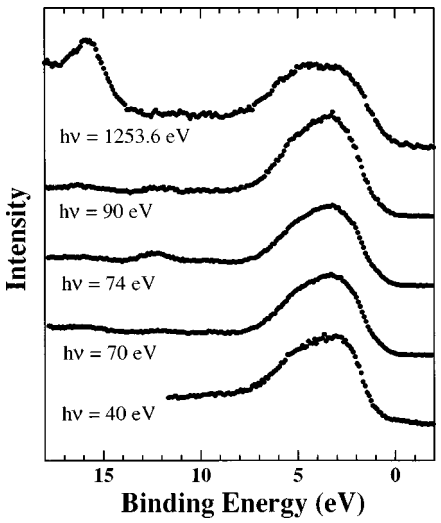

FIG. 3. Valence-band photoemission spectra of $LaCuO_3$ taken at $h\nu=40$, 70, 74, 90, and 1253.6 eV.

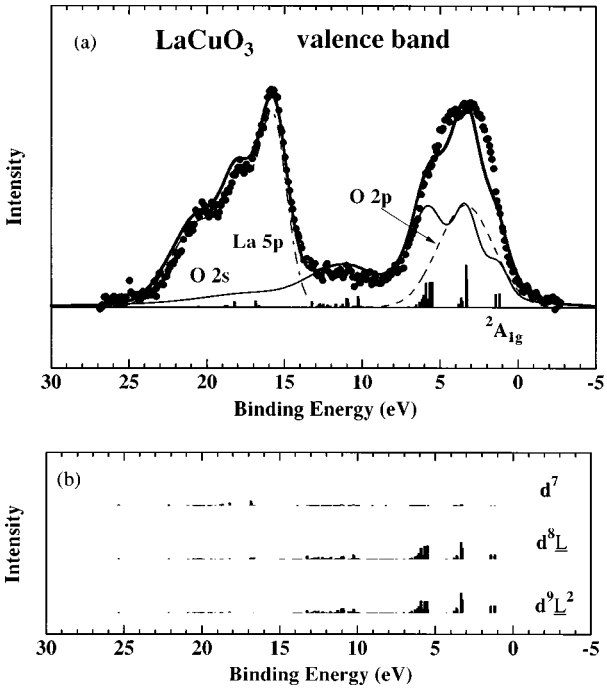

FIG. 4. (a) Cluster-model calculation (thick solid curve) for valence-band photoemission spectra compared with the experimental result ($h\nu=1253.6$ eV) of $LaCuO_3$ (dots). The thin solid curve indicates the contribution from the Cu $3d$ orbitals, which is obtained by broadening the line spectra. (b) The line spectra are decomposed into the configurational components.

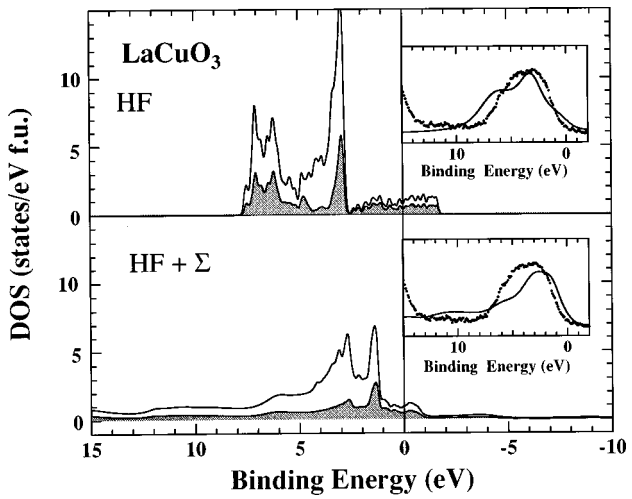

FIG. 5. Spectral function of $LaCuO_3$ calculated using the HF approximation (upper panel) and that including the self-energy correction calculated using the second-order perturbation (lower panel). The shaded area indicates the transition-metal $3d$ spectral weight. In the insets, the calculated results are compared with the valence-band XPS spectrum.

analysis, the final states both of the main-band region from 0 to 8 eV and of the satellite region from 8 to 13 eV are mixtures of the $d^8\underline{L}$ and $d^9\underline{L}^2$ configurations. The first ionization state has ${}^2A_{1g}$ symmetry, which is obtained by emission from the x^2-y^2-type orbitals.

Although the cluster-model calculation gives us an overall picture of the valence-band XPS spectrum including the satellite structure, it is unable to describe the structure near the Fermi level. Here, we are going to interpret the valence-band XPS spectrum of the metallic sample starting from the band-structure calculation. This attempt is meaningful even if the metallic behavior is derived from the small nonstoichiometry. In order to investigate the effect of the translational symmetry of the Cu $3d$ orbitals beyond the single-site cluster model, we have performed HF calculations and subsequent self-energy correction calculations on a Cu $3d$ and O $2p$ lattice model.[26] In this model, the intra-atomic $3d$-$3d$ Coulomb interaction is taken into account in terms of Kanamori parameters, u, u', j, and j', for which the relationships $u'=u-2j$ and $j'=j$ are assumed.[27] These Kanamori parameters are related to Racah parameters through $u=A+4B+3C$ and $j=(5/2)B+C$. The parameters used for the present calculation are $\Delta=0.0$ eV, $U=7.5$ eV, $(pd\sigma)=-1.8$ eV, and $j=0.92$ eV, which are close to those obtained from the cluster-model analyses. In the HF calculation, a G-type AFM insulating state is lower in energy than a paramagnetic (PM) metallic state, contradicting the experimental result. The situation is similar to that found in the LDA+U calculation by Czyzyk and Sawatzky.[12] Here, we are going to compare the density of states of the PM solution with the photoemission spectrum. The HF and self-energy corrected results are shown in Fig. 5. In the insets, the calculated results, where the partial density of states of Cu $3d$ and O $2p$ are multiplied by their photoionization cross section and are broadened with a Gaussian and a Lorentzian, are compared with the experimental results. For the HF result, the FWHM's of the Gaussian and Lorentzian are the same as those for the cluster-model calculation, that is, the Lorentzian is taken to be energy dependent. For the self-energy corrected result, the FWHM of the Lorentzian is fixed at 0.4 eV. The HF solution for the PM metal is essentially the same as that of the LDA calculation.[12,13] In the HF calculation, the broad e_g band, in which the O $2p$ and Cu $3d$ orbitals are strongly hybridized, crosses the Fermi level. As a result, the calculated t_{2g} band is located at ~ 3 eV, which is too deep, and the deviation from the experimental result is large. The HF calculation also fails to reproduce the satellite structure from 8 to 13 eV. In order to calculate the self-energy around the HF solution, we have performed a second-order perturbation expansion in Coulomb interaction using the local approximation, namely, neglecting the momentum dependence of the self-energy. In the self-energy-corrected result, the broad e_g band is strongly renormalized and is narrowed and part of the spectral weight is transferred to the satellite region. However, the band narrowing and the intensity of the satellite structure are too strong, indicating the excessive self-energy correction. In the metallic solution, the screening effect may be important and may have to be taken into account, e.g., through the random phase approximation (RPA). Inclusion of higher-order RPA-type diagrams is expected to weaken the self-energy correction and improve the agreement with the experimental result.

The intensity near the Fermi level, which is overestimated in the HF calculation, is still too strong in the self-energy-corrected spectral function compared with the experimental result. In order to reproduce the intensity at the Fermi level using the self-energy calculation, strong momentum dependence of the self-energy is required. When the momentum dependence of the self-energy is strong and $m_k/m_{\rm HF}$ is much lower than 1, the spectral weight at the Fermi level is multiplied by the factor $m_k/m_{\rm HF}$ and is strongly reduced. Here, $m_{\rm HF}$ is the band mass in the HF calculation and m_k is the so-called k mass defined by[28]

$$m_k/m_{\rm HF}\equiv\frac{\partial\varepsilon_k^{\rm HF}}{\partial k}_{\rm FS}\left(\frac{\partial\varepsilon_k^{\rm HF}}{\partial k}+\frac{\partial\Sigma_k(\omega)}{\partial k}\right)^{-1}_{\rm FS}.$$

$\Sigma_k(\omega)$ is the self-energy and $\varepsilon_k^{\rm HF}$ is the HF energy level. FS represents that the above formula is evaluated on the Fermi surface. In three-dimensional systems, the momentum dependence of the self-energy beyond the local approximation is not so strong as long as the interaction is restricted on the same site.[29] Therefore, it is natural to consider that the insufficiency of the momentum dependence of the self-energy would not be due to the local approximation but would probably be due to the deficit of the d-p lattice model.

C. X-ray-absorption spectra

The O $1s$ XAS spectrum of $LaCuO_3$ is shown in Fig. 6. The peak at ~ 528 eV is mainly derived from the O $2p$ weight hybridized into the unoccupied Cu e_g state. If $LaCuO_3$ is viewed as a 100% hole-doped Cu^{2+} oxide, the peak corresponds to that growing with hole doping in the pre-edge region of $La_{2-x}Sr_xCuO_4$.[4] The structures ranging from 530 to 545 eV are due to the La $4f$,$5d$ and Cu $4s$,$4p$ states. In Fig. 7, the Cu $2p$ XAS spectrum is compared with the CuO_6 cluster-model calculation using the parameter set for Cu $2p$ XPS. From the local-cluster viewpoint, the $2p_{3/2}$

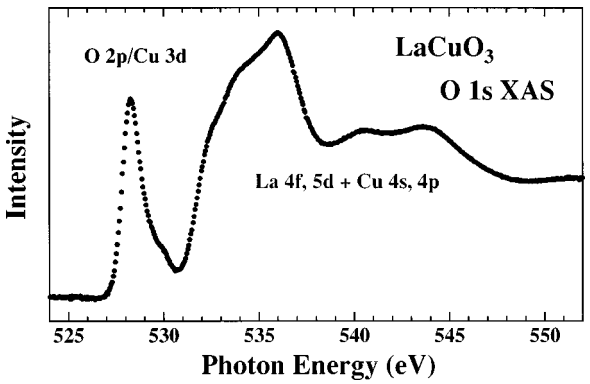

FIG. 6. O 1*s* XAS spectrum of $LaCuO_3$.

and $2p_{1/2}$ main peaks located at ~931 and ~951 eV, respectively, have $\underline{c}d^{10}\underline{L}$ character and the broad satellite structures at ~940 and ~960 eV to have $\underline{c}d^9$ character. However, the $2p_{3/2}$ and $2p_{1/2}$ main peaks are split into two structures, which makes it impossible to fit the Cu $2p$ XAS spectrum by the single-site cluster-model calculation. Let us denote these structures as A, A', B, and B', respectively, as shown in Fig. 7. Sarma *et al.*[6] and Chen *et al.*[30] have observed that the new structure, which is located at ~2 eV higher energy than the main peak, grows as an insulating Cu^{2+} oxide is hole doped. van Veenendaal and Sawatzky have calculated the Cu $2p$ XAS for 50% hole-doped Cu^{2+} oxide using a two-site cluster model and have shown that a new structure, in which the intercluster screening effect is weak, appears on the high-energy side of the main structure, in which the intercluster screening effect is strong.[24] Very recently, Okada and Kotani have calculated the Cu $2p$ XAS and XPS spectra for Cu^{3+} oxide or 100% hole-doped Cu^{2+} oxide using a multisite cluster model with a 180° Cu-O-Cu bond angle and have found that the main peak is split into two structures in Cu $2p$ XAS and is almost single in Cu $2p$ XPS.[31] Therefore, it is natural to consider that structures A and A' are derived from the states strongly screened by intercluster interaction and structures B and B' from those weakly screened. The Cu $2p$ XAS spectrum suggests that the intercluster interaction is very strong in $LaCuO_3$, which has a 180° Cu-O-Cu bond angle. When the intersite interaction is weak, the splitting between

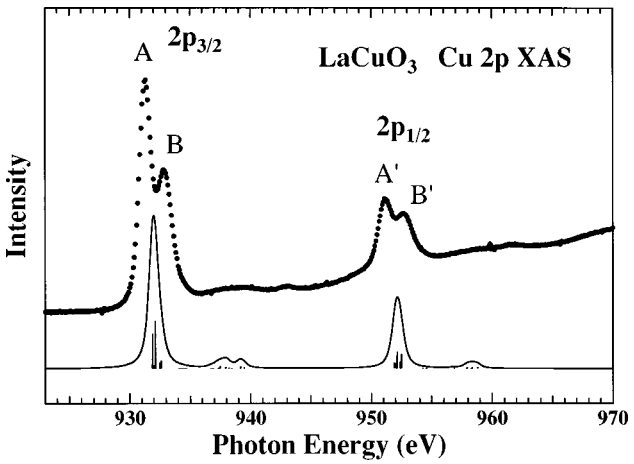

FIG. 7. Cu $2p$ XAS spectrum of $LaCuO_3$ (dots) compared with the cluster-model calculation (solid curve).

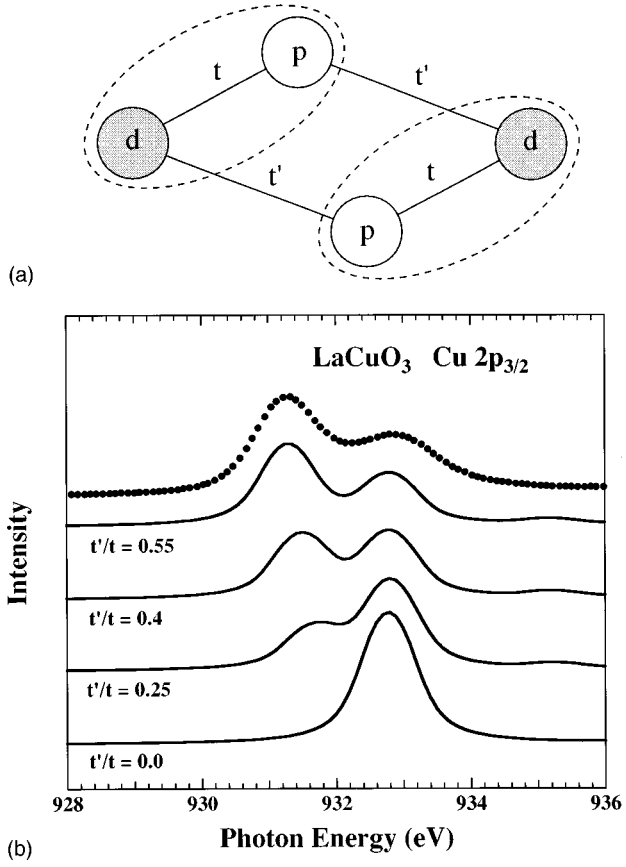

FIG. 8. (a) A schematic drawing of the two-site cluster model. (b) Cu $2p$ XAS spectra of $LaCuO_3$ (dots) compared with the two-site cluster-model calculations (solid curves).

A (A') and B (B') is expected to disappear.[24] Actually, in $NaCuO_2$, which has a 90° Cu-O-Cu bond angle, the Cu $2p_{3/2}$ and $2p_{1/2}$ main peaks are almost single peaks.[6]

In order to investigate the effect of the intercluster interaction, we have considered a two-site cluster model, where two Cu $3d$ sites and two O $2p$ sites are included. In the present model, a hole on each O $2p$ site can be transferred to the Cu $3d$ site in the same cluster with transfer integral t and to the other Cu $3d$ site with t' ($t>t'$) as shown in Fig. 8(a). The ratio t'/t shows the strength of the intercluster interaction. The degeneracy of the $3d$ orbitals and the multiplet coupling is neglected. The values for Δ, U, Q are fixed to -2, 7, and 11 eV, respectively. In order to reproduce the energy separation between the two peaks, we had to introduce another parameter V_{cp}, which can be viewed as the Coulomb interaction between a Cu $2p$ core hole and an O $2p$ hole within a cluster. While the effect of V_{cp} can effectively be included in Q for the single-site model, it is relevant for the two-site model. With $t=1.5$ eV, $V_{cp}=1.8$ eV and $t'/t=0.55$, the double-peak structure of the Cu $2p_{3/2}$ XAS for tetragonal $LaCuO_3$ is well reproduced as shown in Fig. 8(b). The value of V_{cp} is too large for intersite Coulomb interaction. This is probably because the present two-site model is too simplified and fails to include some intercluster interaction. The final state for the well-screened peak is dominated by the configuration where the two holes are located at one O site. Here, the O site belongs to the cluster without the Cu $2p$ core hole. On the other hand, in the well-

screened state, the weight of the configuration where the two ligand holes are distributed to the two O sites is enhanced. With decreasing t'/t, the intensity ratio of the well-screened peak to the poorly screened one becomes smaller and the main peak of Cu $2p_{3/2}$ XAS becomes single for $t'/t=0.0$.

IV. CONCLUSION

We have investigated the electronic structure of $LaCuO_3$ by means of photoemission and x-ray-absorption spectroscopy. The charge-transfer satellite observed in the valence-band and Cu $2p$ core-level photoemission spectra allow us to apply the CI cluster-model analyses to $LaCuO_3$. From the analyses, the charge-transfer energy is estimated to be ~ -1 eV and the ground state mainly has $d^9\underline{L}$ character although in the ground state the d^8 configuration is strongly hybridized into the $d^9\underline{L}$ configuration. The Cu $2p$ XAS spectrum, which cannot be explained by the single-site cluster-model calculation, shows the importance of the intercluster interaction in $LaCuO_3$. In order to understand the XAS spectra of $LaCuO_3$, we have performed two-site cluster-model calculations. These experimental results and analyses show that $LaCuO_3$, which has an almost 180° Cu-O-Cu bond angle, is accompanied by the strong intercluster interaction, which is in contrast to $NaCuO_2$ with 90° Cu-O-Cu bond angle. The strong intercluster interaction in $LaCuO_3$ is expected to reduce the magnitude of the band gap compared with $NaCuO_2$. However, it should be noted that we cannot determine from the present photoemission measurement which of the strong intercluster interactions and the small deviation from the stoichiometry is responsible for the metallic behavior of $LaCuO_3$ since it is impossible to confirm the stoichiometry of the sample with an accuracy less than 1%. Even if stoichiometric $LaCuO_3$ is an AFM insulator and a small amount of oxygen deficiency makes it metallic, it may be due to the 180° Cu-O-Cu bond angle that the small amount of electron doping by oxygen deficiency makes it metallic.

We have also performed the HF and subsequent self-energy calculations on the Cu $3d-$O $2p$ lattice models using the electronic-structure parameters obtained from the cluster-model analysis of the photoemission spectra. The valence-band photoemission spectra including the satellite structure is to some extent reproduced but the weak spectral intensity near the Fermi level compared with the band-structure calculation cannot be explained by the second-order perturbation calculation of the self-energy. Although the AFM insulating solution has the lowest energy in the HF and LDA+U calculations,[12] the fluctuation around the mean-field solutions may make the PM metallic state lower in energy than the AFM insulating state. Further study along these lines should be made in the future.

ACKNOWLEDGMENTS

The authors would like to thank A. Yagishita and the staff of Photon Factory for technical support in the XAS measurements. They also thank S. Shin, Y. Tezuka, and the staff of Synchrotron Radiation Laboratory for technical support in the UPS measurements. They are grateful to K. Morikawa, T. Saitoh, A. Sekiyama, I. H. Inoue, M. Nakamura, and S. Nohara for assistance in the XAS and UPS measurements. Part of the calculations in this work were performed on a VAX computer in Meson Science Laboratory, Faculty of Science, University of Tokyo. The present work was supported by a Grant-in-Aid for Scientific Research from the Ministry of Education, Science and Culture and by the New Energy and Industrial Technology Development Organization (NEDO). Part of this work has been done under the approval of the Photon Factory Program Advisory Committee (Proposal No. 94G361).

[1] J. G. Bednorz and K. A. Müller, Z. Phys. B **64**, 189 (1986).
[2] A. Fujimori, E. Takayama-Muromachi, Y. Uchida, and B. Okai, Phys. Rev. B **35**, 8814 (1987).
[3] Z.-X. Shen, J. W. Allen, J. J. Yeh, J.-S. Kang, W. Ellis, W. Spicer, I. Lindau, M. B. Maple, Y. D. Dalichaouch, M. S. Torikachvili, and J. Z. Sun, Phys. Rev. B **36**, 8414 (1987).
[4] C. T. Chen, F. Sette, Y. Ma, M. S. Hybertsen, E. B. Stechel, W. M. C. Foulkes, M. Schluter, S-W. Cheong, A. S. Cooper, L. W. Rupp, Jr., B. Batlogg, Y. L. Soo, Z. H. Ming, A. Krol, and Y. H. Kao, Phys. Rev. Lett. **66**, 104 (1991).
[5] P. Steiner, V. Kinsinger, I. Sander, B. Siegwart, S. Hufner, C. Politis, R. Hoppe, and H. P. Muller, Z. Phys. B **67**, 497 (1987).
[6] D. D. Sarma, O. Strebel, C. T. Simmons, U. Neukirch, G. Kaindl, R. Hoppe, and H. P. Muller, Phys. Rev. B **37**, 9784 (1988).
[7] T. Mizokawa, H. Namatame, A. Fujimori, K. Akeyama, H. Kondoh, H. Kuroda, and N. Kosugi, Phys. Rev. Lett. **67**, 1638 (1991); **70**, 1565(E) (1993); T. Mizokawa, H. Namatame, A. Fujimori, K. Akeyama, H. Kondoh, H. Kuroda, and N. Kosugi, Phys. Rev. B **49**, 7193 (1994).
[8] G. Demazeau, C. Parent, M. Pouchard, and P. Hagenmuller, MRS Bull. **7**, 913 (1972).
[9] J. F. Bringley, B. A. Scott, S. J. La Placa, R. F. Boehme, T. M. Shaw, M. W. McElfresh, S. S. Trail, and D. E. Cox, Nature (London) **347**, 263 (1990).
[10] J. F. Bringley, B. A. Scott, S. J. La Placa, T. R. McGuire, F. Mehran, M. W. McElfresh, and D. E. Cox, Phys. Rev. B **47**, 15 269 (1993).
[11] S. Drracq, S. Matar, and G. Demazeau, Solid State Commun. **85**, 961 (1993).
[12] M. T. Czyzyk and G. A. Sawatzky, Phys. Rev. B **49**, 14 211 (1994).
[13] N. Hamada, H. Sawada, and K. Terakura, in *Spectroscopy of Mott Insulators and Correlated Metals*, edited by A. Fujimori and Y. Tokura (Springer-Verlag, Berlin, 1995), p. 95.
[14] M. Abbate, F. M. F. de Groot, J. C. Fuggle, A. Fujimori, O. Strebel, F. Lopez, M. Domke, G. Kaindl, G. A. Sawatzky, M. Takano, Y. Takeda, H. Eisaki, and S. Uchida, Phys. Rev. B **46**, 3771 (1992).
[15] M. Grioni, J. B. Goedkoop, R. Schoorl, F. M. F. de Groot, J. C. Fuggle, F. Schäfers, E. E. Koch, G. Rossi, J.-M. Esteva, and R. C. Karnatak, Phys. Rev. B **39**, 1541 (1989).
[16] J. Ghijsen, L. H. Tjeng, J. van Elp, H. Eskes, J. Westerink, G. A. Sawatzky, and M. T. Czyzyk, Phys. Rev. B **38**, 11 322 (1988).
[17] J. Zaanen, C. Westra, and G. A. Sawatzky, Phys. Rev. B **33**, 8060 (1986).

[18] K. Okada and A. Kotani, J. Phys. Soc. Jpn. **60**, 772 (1991); **61**, 4619 (1992).
[19] J. C. Slater and G. F. Koster, Phys. Rev. **94**, 1498 (1954).
[20] L. F. Mattheiss, Phys. Rev. B **5**, 290 (1972).
[21] W. A. Harrison, *Electronic Structure and the Properties of Solids* (Dover, New York, 1989).
[22] F. M. F. de Groot, M. Grioni, J. C. Fuggle, J. Ghijsen, G. A. Sawatzky, and H. Petersen, Phys. Rev. B **40**, 5715 (1989).
[23] A. E. Bocquet, A. Fujimori, T. Mizokawa, T. Saitoh, H. Namatame, S. Suga, N. Kimizuka, Y. Takeda, and M. Takano, Phys. Rev. B **45**, 1561 (1992).
[24] M. A. van Veenendaal and G. A. Sawatzky, Phys. Rev. B **49**, 3473 (1994).
[25] G. A. Sawatzky and D. Post, Phys. Rev. B **20**, 1546 (1979); J. J. Yeh and I. Lindau, At. Data Nucl. Data Tables **32**, 1 (1985).
[26] T. Mizokawa and A. Fujimori, Phys. Rev. B **51**, 12 880 (1995); **54**, 5368 (1996).
[27] J. Kanamori, Prog. Theor. Phys. **30**, 275 (1963).
[28] G. D. Mahan, *Many Particle Physics* (Plenum, New York, 1981); C. W. Greeff, H. R. Glyde, and B. E. Clements, Phys. Rev. B **45**, 7951 (1992).
[29] H. Schweitzer and G. Czycholl, Solid State Commun. **74**, 735 (1990).
[30] C. T. Chen, L. H. Tjeng, J. Kwo, H. L. Kao, P. Rudolf, F. Sette, and R. M. Fleming, Phys. Rev. Lett. **68**, 2543 (1992).
[31] Kozo Okada and Akio Kotani (unpublished).